AIAA JOURNAL
Vol. 41, No. 8, August 2003

Atomic Oxygen Degradation of Polymeric Thin Films in Low Earth Orbit

G. Allegri,* S. Corradi,† and M. Marchetti‡
University of Rome "La Sapienza," 00184 Rome, Italy
and
V. Milinchuck§
Obninsk's Institute of Nuclear Power Engineering, 249020, Obninsk, Russia

A Monte Carlo simulation technique to evaluate the effects of low-Earth-orbit atomic oxygen damage on thin films of polymeric materials is presented and discussed. The proposed method provides a tool that allows the evaluation of both the mean eroded thickness for exposed specimens and the degradation of their optical properties. Contrary to a full quantum mechanics approach, this method is based on a finite volume discretization of the bulk materials: Each simulation cell is characterized by a reaction probability in a standard exponential form. The reaction probability depends on the ratio between the total amount of kinetic energy transferred to the finite volume by the entering atomic flux and the internal pressure, that is, the cohesive energy of the simulation cell itself. The unknown parameters contained in the expression of the reaction probability are related to the mean eroded thickness and to the surface roughness rms through statistical considerations. The erosion yield is shown to be dependent on the cohesive energy density for polymeric materials: This observation provides a simple tool to estimate the reaction yields for standard hydrocarbon or fluoro-based polymers. The surface roughness rms is obtained from the mean optical properties of exposed materials via the scalar equations describing electromagnetic wave surface scattering. The results of Monte Carlo simulations have been compared to the data available for Kapton® specimens flown both on the Long Duration Exposure Facility and Mir and retrieved after several months of exposition. The unknown parameters required for the simulations have been estimated by a nonlinear regression on experimental data. Good agreement has been obtained between the simulation results and the experimental data, both for the eroded thickness after exposure and for the mean optical transmittance of the specimens.

Nomenclature

E = Young's modulus
p = pressure
T = temperature
V = volume
α = coefficient of thermal expansion
ν = Poisson's modulus

I. Introduction

DIRECT exposition to the near-Earth space environment causes profound alterations of the thermal, mechanical, and optical properties of flown materials: These effects typically depend on synergistic interactions between the spacecraft and the different elements of the space environment itself, such as neutral gas, plasma, and radiation, as well as micrometeoroids and debris. The specific entity and nature of the interactions is related both to the orbit of the spacecraft and to the materials employed. The action of neutral gas is largely dominant for the low-Earth-orbit (LEO) environment, which ranges from an altitude of 200–1000 km and from an inclination of 0–60 deg above the equatorial plane.

Received 30 April 2002; revision received 15 November 2002; accepted for publication 22 January 2003.

*Research Scientist, Department of Aerospace and Astronautical Engineering; allegri@aerorisc.ing.uniroma1.it. Student Member AIAA.
†Research Scientist, Department of Aerospace and Astronautical Engineering; corradi@aerorisc.ing.uniroma1.it.
‡Full Professor, Department of Aerospace and Astronautical Engineering; marchett@aerorisc.ing.uniroma1.it.
§Full Professor; milinchuk@iate.obninsk.ru.

Atomic oxygen (AO) is the most abundant element present in the neutral gas environment, characterizing the LEO environment. Since the Skylab mission and the early space shuttle (SST) flights, it has been highlighted that AO can produce damaging erosion of exposed surfaces, especially for polymeric materials.[1] This effect depends mainly on the relative velocity of AO atoms impacting the spacecraft, which is about 8 km/s, corresponding to a total kinetic energy of 5 eV. This level is sufficient to break covalent chemical bonds, particularly in the case of hydrocarbon polymers. Several in situ[2–5] and laboratory[6] tests have been carried out on samples of different materials, to assess the effects of AO attack, which usually produces superficial erosion and, therefore, a sensible mass loss in the exposed specimens. The AO erosion is augmented by several factors,[7,8] typically acting in synergistic interaction, such as solar UV irradiation, proton and electron radiation, thermal cycling, and contamination in high vacuum conditions typical of near-Earth orbits. The main consequences of AO erosion are the degradation of the thermal, mechanical, and optical properties characteristic of the exposed materials.[9–11] These effects can be very severe, leading to the failure of the entire mission, and, therefore, they must be taken into consideration in the design stage.

Early analyses of the effect of AO erosion on space-exposed materials have been focused on the development of engineering tools for a simple and reliable modeling of the effects of the neutral gas attack. Namely, the mass and thickness loss have been assumed proportional to the total time integrated flux of AO impacting the exposed surfaces,[1] that is, the total fluence. The SPENVIS[12] simulation package is an online tool provided by ESA, whose ATOMOX routine allows estimation of the total fluence of neutral gas affecting a spacecraft during its mission. The computation of neutral eterosphere composition is achieved by the standard MSIS-90 model,[12] whereas the erosion depth due to AO attack for exposed materials is evaluated through the calculation of the total fluence accumulated during the spacecraft mission. A database of AO reactivity values for several materials (i.e., the experimental proportional parameter

of erosion depth vs AO fluence) is currently available online at the SPENVIS home page.[13]

As already underlined by many scientists, several synergistic effects can contribute to AO degradation of exposed materials: Nevertheless, each material shows a typical sensibility to specific interactions, which can augment the action of the neutral gas. Namely, the erosion of metallic and metallic oxides is strongly dependent on thermal cycling, on superficial contamination, and also on radiation damage. Moreover, hypervelocity impacts with space debris and micrometeroids can produce microholes and vents on the exposed specimens that constitute optimal sites for the onset of the AO attack. As the main consequence, all of the synergistic effects already discussed are characterized by nonlinearities in the erosion process. This makes the description of this phenomenon more difficult, so that although several in situ missions and surveys have been performed to provide information on erosion rates, there is still a considerable number of parameters characterizing the operative environment of exposed specimens whose effects have not yet been fully understood. Some tests have highlighted a dependence of the erosion rates on the temperature of the samples, which periodically varies along the orbit due to the alternation of direct sunlight and shadow: This dependence is expected because the chemical reactivity of the material to AO should be ruled by an Arrenhius type law, even if the actual entity of the temperature effect is still to be quantified.

Laboratory and in situ tests have also highlighted the dependence of the reaction rates on the attitude of the exposed specimens. This effect is partly described by the concept of fluence itself because the AO flux depends on the cosine of the angle between the normal to the surface and the velocity vector. However, for Kapton® and Mylar® specimens,[14–16] it has been observed that the reaction yield depends on the cosine of the angle between the surface normal and the velocity of the AO stream raised to the 1.5 power. Nevertheless, because this effect has been measured only on a very limited set of experimental data, it is usually neglected by commonly employed AO interaction simulators, such as the ATOMOX[12] tool of the SPENVIS package developed by ESA. The standard reaction yield is, therefore, referred to normal incidence expositions for surveyed materials. The attitude of the specimens is taken into consideration only for the calculation of the impinging flux and fluence.

Some Monte Carlo modeling techniques have been proposed to evaluate the materials reactivity vs the atomic oxygen irradiation.[1,7,17,18] These models have been based on a complete representation of the interactions between an impinging AO flux and the bulk material, that is, scattering without chemical reaction, recombination to form nonreactive O_2, and production of volatile oxides.[1] The probability of these latter events must be known a priori to develop a reliable modeling of hyperthermal AO attack.[7] Furthermore, ray-tracing procedures have been combined with Monte Carlo analysis to describe the oxygen atoms trajectories within the material: According to the Banks,[1] Banks et al.,[17] and Snyder and Banks[18] model, impinging AO atoms can be grouped into equivalent Monte Carlo reactive particles that interact with the finite volume simulation cells. Note that, even though the approaches developed thus far can provide clear understanding of the AO erosion phenomena from a purely physical point of view, they are time and cost consuming because they require access to powerful computers. The basic aim of this paper is to provide a fast, simple, reliable technique to model the interactions of AO with polymeric materials. The approach here presented is still based on a Monte Carlo simulation strategy, even though the bulk material is discretized in microscopic simulation cells and the detailed atomic and molecular structure of the attacked polymer discarded, as developed by Banks.[1] The proposed method has the main advantage of relating both the erosion rates and the degradation of the optical properties of the exposed polymers to the AO fluence as a consequence of an assigned mission profile. The model is validated by consideration of the results of experimental surveys performed on specimens retrieved after in situ exposition both on the Long Duration Exposure Facility (LDEF) and Mir missions. Validation of the model is centered around the degradation of exposed Kapton thin films.

II. Analysis of Kapton Films Exposed on LDEF and Mir: Experimental Results

Both the LDEF and Mir missions have been designed for exposing samples of several materials to the LEO environment. Postflight experimental investigations have highlighted a sensible reduction of the thickness of the exposed samples and a strong alteration of their thermooptical properties. A summary of the final geometric and optical properties of exposed unprotected Kapton HN films flown both on LDEF and Mir is presented in Table 1: The spectral range considered for the experimental analysis is 550–900 nm (Kapton transmittance drops down below 550 nm), corresponding to a portion of the visible electromagnetic radiation, near infrared.

The Kapton films exposed on LDEF were initially 125 μm thick. The specimens exposed for 10 months were placed at the trailing edge of the satellite. The total AO fluence for these samples has been evaluated by the ATOMOX tool of the SPENVIS space environment analysis suite, with consideration of the data concerning solar activity during the first 10 months of LDEF missions, from April 1984 to February 1985, when the specimens were retrieved by SST.[2,3] The eroded thickness has been evaluated under the assumption of a reaction yield $R = 3.0 \times 10^{-30}$ atoms/m^3 for Kapton HN. The initial orbit of LDEF was circular, at an altitude of 509 km and an inclination of 28.4 deg to the equatorial plane. During its mission, which lasted 5.7 years (about 70 months), the LDEF altitude decreased progressively to 324 km due to atmospheric drag. Therefore, the AO fluence accumulated during the last year of flight represents about 75% of the total exposure for the LDEF mission. Because the LDEF attitude was pitched at about 8 deg, the space end of the satellite received a total amount of AO fluence, which was about 5% of that characterizing the LDEF trailing edge. Therefore, the total fluence for specimens exposed during the entire 68-month mission is only twice that for samples flown 10 months. The total eroded thickness has also been evaluated for specimens exposed for 68 months by consideration of a reaction yield $R = 3.0 \times 10^{-30}$ atoms/m^3.

For the Mir exposed specimens, which had an initial thickness of 25 μm, the first experiment lasted 28 months, from July 1995 to November 1997, whereas the second experiment lasted 42 months, from July 1995 to January 1999. Because no data are provided about the orientation of the specimens flown on the Mir station, a SPENVIS simulation has been performed to estimate the total leading-edge fluence. Moreover, the total fluence of AO for the exposed specimens has also been evaluated by division of the experimentally assessed eroded thickness by the Kapton reaction yield. This value and the result of the SPENVIS analysis differ by an order of magnitude, thus, highlighting that the specimens surface had been oriented nearly parallel to the velocity vector and toward the

Table 1 Summary of experimental data for Kapton HN films flown on LDEF and Mir

Mission	Duration, months	Location	Fluence, atoms/m^2	Eroded thickness, m	Initial mean transmittance, %	Final mean transmittance, %
LDEF	10	Trailing edge	1.79×10^{24} [a]	5.4×10^{-6} [b]	78	25
LDEF	68	Space end	4.27×10^{24}	12.8×10^{-6} [b]	70	8
Mir	28	——	2.33×10^{24} [c]	7×10^{-6}	77	6
Mir	42	——	5.33×10^{24} [c]	16×10^{-6}	77	3

[a]Fluence estimated by SPENVIS simulation.
[b]Eroded thickness evaluated by assumption that $R = 3.0 \times 10^{-30}$ atoms/m^3 for Kapton HN.
[c]Fluence estimated by assumption that $R = 3.0 \times 10^{-30}$ atoms/m^3 for Kapton HN.

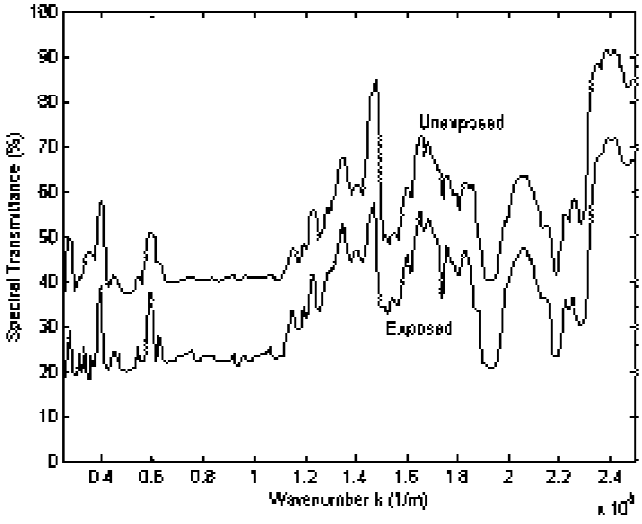

Fig. 1 Effect of combined AO and UV exposition on LDEF Kapton film specimens after 70-month exposure (data from Ref. 2).

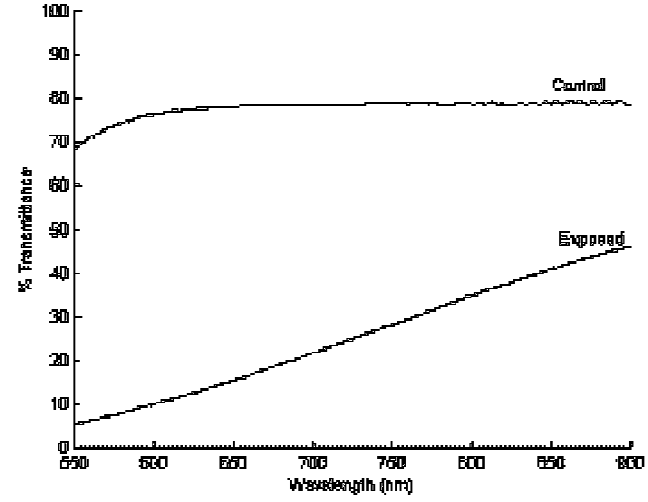

Fig. 2 Experimental transmittance spectrum for LDEF specimens: 10-month exposure, data from Ref. 2.

space side, with direct UV irradiation. The different fluence rates for the 28- and 42-month flights are related to the fluctuations in solar activity during the Mir mission because the orbit of the station had been held at a constant altitude of 400 km by periodical reboosts. The inclination of the Mir orbit was 51.6 deg to the Earth equatorial plane.

The optical properties of the exposed Kapton films appear to be strongly reduced. Table 1 shows a clear correlation between the total AO fluence and the entity of transmittance reduction beyond 550 nm. Even though these effects have been thus far related mainly to surface roughness, it is worth investigating whether any synergistic interactions of AO bombardment with UV radiation can contribute to the transmittance reduction in the 550–900-nm range. In fact, LDEF specimens had been exposed to 14,500 equivalent sun hours (ESH). Moreover, though no reliable data are available about total sunlight irradiation of Mir exposed specimens, it should be expected that they have experienced an electromagnetic irradiation comparable to those of LDEF. If synergistic interactions between AO and UV radiation occurred, they would have altered the chemical composition of the polymer, providing significant changes in the transmittance spectrum, with particular emphasis in the infrared range.

Nevertheless, as shown in Fig. 1, the infrared transmittance spectrum for the LDEF exposed Kapton, given the working precision of the spectrophotometer employed, does not exhibit any sensible phase shift or peak alteration, showing that no chemical modification has affected the polymer during its exposure to combined AO flux and UV radiation. In fact, the transmittance spectrum appears to be simply shifted toward lower values. Therefore, the decrease in transmittance, observed both in LDEF and Mir specimens, is related only to the surface roughening due to AO erosion.

This result is also confirmed by previous works[2,3] on Kapton film in situ exposure, which have already demonstrated that this material is insensitive to UV radiation.

The spectra for the specimens exposed both on LDEF and on Mir are presented in Figs. 2–5, which report experimental data.[1,2,19] LDEF specimens geometry were circular disks (3-cm diam) made of Kapton, rigidly fixed on a metallic substrate, whereas Mir specimens were rectangular thin plates (5 × 6 cm) fixed to metallic rigid frames. It can be observed that the reduction of transmittance affects the whole wavelength range considered here, though the difference between the spectra of exposed and unexposed specimens decreases at increasing λ. This latter effect is undoubtedly related to the increase in surface roughness.

As was already underlined, the transmittance decrease is related to the total amount of AO fluence for flown specimens. This observation is further confirmed by analysis of the Kapton film spectra reported here because the transmittance loss is lower for the 10-month flown specimens than for all others.

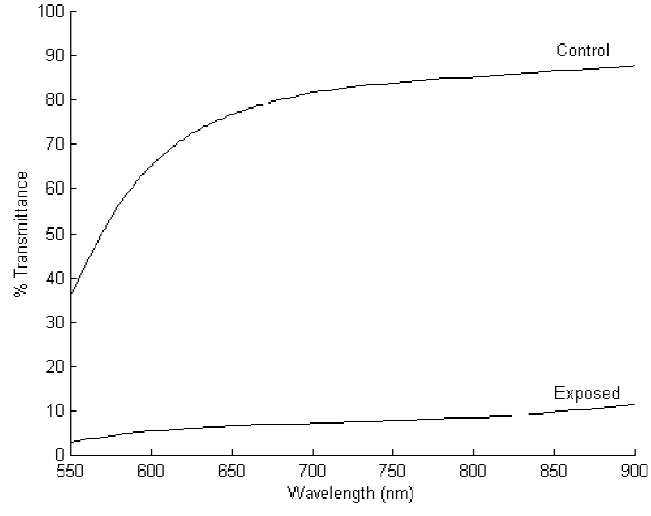

Fig. 3 Experimental transmittance spectrum for Mir specimens: 28-month exposure, data from Ref. 13.

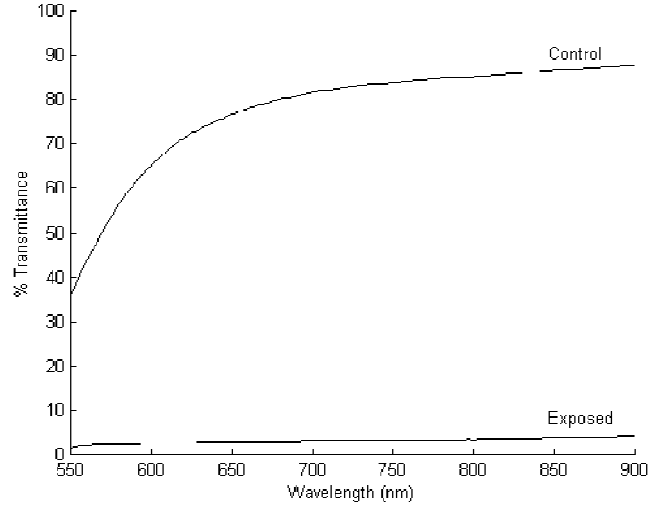

Fig. 4 Experimental transmittance spectrum for Mir specimens: 42-month exposure, data from Ref. 13.

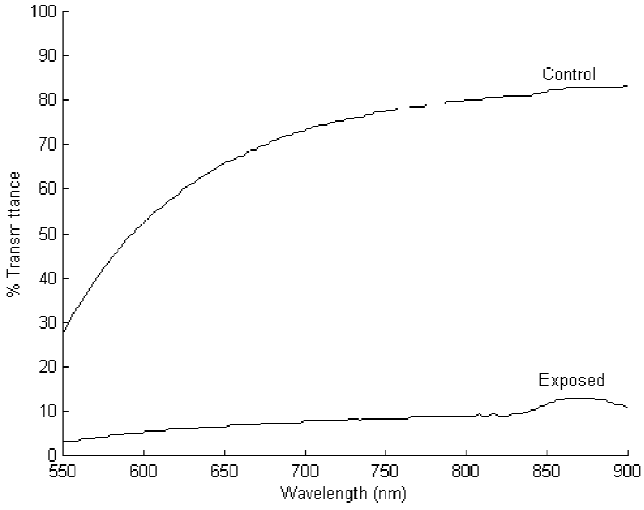

Fig. 5 Experimental transmittance spectrum for LDEF specimens: 70-month exposure, data from Ref. 2.

The residual transmittance for Mir specimens is very low and apparently stable after 28 months of exposure.[19] However, these experimental data are not fully reliable because the sensibility threshold of the spectrophotometer employed by the Russian researcher was about 5% and the measurement error was about ±1% (Ref. 19).

The Kapton film transmittance spectrum for the specimens exposed on LDEF for 70 months differs slightly from the others presented here: The initial transmittance is lower, and the final spectrum shows a local maximum about 870 nm, as shown in Fig. 5. This latter effect can be explained neither by considerations about the evolution of surface roughness, nor by measurement error because the transmittance was surveyed several times and the spectrophotometer employed was the same used in the case of 10-month exposed specimens. The transmittance increase, which appears only in a very narrow band of the spectrum, is probably related to the presence of some contaminant substances during the final stage of the LDEF mission, when the action of the neutral atmosphere was particularly intense.[2]

III. Simulation of AO Erosion

Let us assume that a representative volume of material is split into equal rectangular shaped cells, as shown in Fig. 6, whose length and width are each represented by d and whose thickness is given by h. The reaction probability for each cell exposed to the normal AO flux has the standard exponential form

$$p_{rn} = k_r \exp -(E_i / E_{f,\Delta t}) \tag{1}$$

where E_i is the energy required for chemical interactions to occur, $E_{f,\Delta t}$ is the mean value of total kinetic energy stored in each cell by the AO flux during an assigned time interval Δt, and k_r is a reaction constant that will be shown to be related to both the interaction energy E_i and the cell thickness h. The difference between the total kinetic energy of the impinging flux and the energy stored in the cell volume by surface accomodation is accounted for by the reaction constant k_r, which is experimentally evaluated through in situ tests. Consequently, Eq. (1) differs from an Arrhenius type law utilized for the reaction probability, such as that employed by Banks.[1]

The mean value of the total energy transported by the AO flux is given by the expression

$$E_{f,\Delta t} = \tfrac{1}{2} m_0 \overline{v^2} F_{\Delta t} d^2 \tag{2}$$

where $m_0 = 2.657 \times 10^{-26}$ is the mass of an oxygen atom, $F_{\Delta t}$ is the AO fluence evaluated over the time interval Δt, and $\overline{v^2}$ is the mean quadratic velocity of the flux. Note that $\bar{v}^2$ given by the sum of the squared orbital velocity v_{orb} and the mean quadratic value of

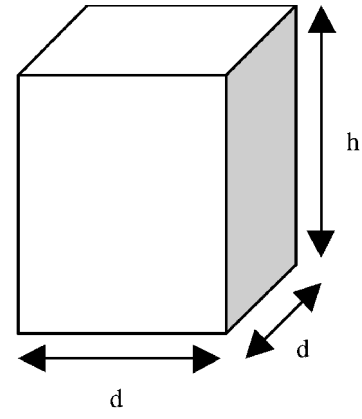

Fig. 6 Prismatic cell for Monte Carlo simulations of AO attack.

the random thermal motion velocities; therefore, it has the following expression:

$$\overline{v^2} = v_{\text{orb}}^2 + 3(kT_g / m_0) \tag{3}$$

where k is the Boltzmann constant and T_g is the absolute temperature of the neutral gas. For the interaction energy E_i, let us introduce the following expression:

$$E_i = \omega_i d^2 h \tag{4}$$

where ω_i is the interaction energy density, calculated for 1 m^3 of bulk material. Generally, the interaction energy represents the magnitude of the total kinetic power that must be transferred to the material to have a significant probability of chemical interaction with the AO impinging flux. The values of E_i for a specific material are closely dependent on its composition. The estimation of the interaction energy density ω_i will be discussed in Sec. IV.

Substituting the expressions (2) and (4) into Eq. (1) yields the following form for the reaction probability of a finite volume of material:

$$p_{rn} = k_r \exp -\left(\frac{2\omega_i}{m_0 \overline{v^2} F_{\Delta t}} \right) h \tag{5}$$

which depends only on the thickness h of the simulation cells.

Let us consider a monodimensional array of N simulation cells hit by a normal AO flux, directed along the z axis (Fig. 7), where N is a sufficiently large integer number. The array just described coincides with the first row of the matrix of simulation cells shown in Fig. 7 according to expression (5). For each cell, there is a finite probability of being eroded. For this set of finite volumes, the mean eroded thickness can be evaluated as

$$\bar{\delta} = (\delta_1 + \delta_2 + \cdots + \delta_N)/N = N_r h / N = p_{rn} h \tag{6}$$

where δ_i is the eroded thickness for each cell. Assuming that we discretize the oxygen etching process, each finite simulation volume can either survive or be completely eroded, so that the total amount of thickness lost is simply given by the product of the number N_r of etched cells and of their dimension h. The ratio between the latter quantity and the total number of cells gives the mean value of the eroded thickness, and, given that $N_r / N = p_{rn}$ for $N \to \infty$, it yields Eq. (6). When the same steps are followed, it is easy to show that the mean quadratic value of the thickness lost is given by

$$\overline{\delta^2} = \left(\delta_1^2 + \delta_2^2 + \cdots + \delta_N^2\right) \Big/ N = N_r h^2 \Big/ N = p_{rn} h^2 \tag{7}$$

The standard deviation σ_δ of a random variable δ is defined as

$$\sigma_\delta^2 = \overline{\delta^2} - \bar{\delta}^2 \tag{8}$$

and so the substitution of Eqs. (6) and (7) into Eq. (8) yields

$$h^2 p_{rn}(1 - p_{rn}) = \sigma_\delta^2 \tag{9}$$

Equations (6) and (9) constitute a nonlinear system whose unknown quantities are the thickness of the simulation cells and the reaction

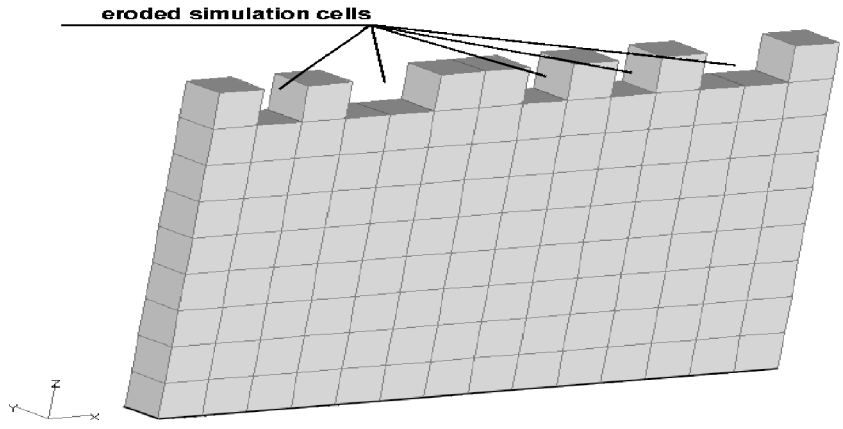

Fig. 7 Array of finite volume for Monte Carlo simulations of AO attack: two-dimensional discretization of the bulk material.

constant k_r, provided that the interaction energy density ω_i has been evaluated (Sec. IV), and that the AO fluence $F_{\Delta t}$ and the temperature T have been assigned. Under the assumption that

$$\beta = 2\omega_i \big/ m_0 \overline{v^2} F_{\Delta t} \tag{10}$$

Eqs. (6) and (9) can be rearranged in the following form:

$$hk_r e^{-\beta h} = \overline{\delta_{\Delta t}}, \qquad h^2 k_r e^{-\beta h}\left(1 - k_r e^{-\beta h}\right) = \sigma^2_{\delta,\Delta t} \tag{11}$$

where $\beta > 0$ and the subscript Δt refers to the time discretization.

The nonlinear system (11) can easily be solved by simple algebraic passages that yield

$$k_r = \left(\overline{\delta_{\Delta t}} \big/ h\right) e^{\beta h}, \qquad h = \overline{\delta_{\Delta t}} + \sigma^2_{\delta,\Delta t} \big/ \overline{\delta_{\Delta t}} \tag{12}$$

When the standard approaches to model AO erosion of materials are followed, the mean eroded thickness can be expressed as a function of the total fluence $F_{\Delta t}$, resulting in

$$\overline{\delta_{\Delta t}} = F_{\Delta t} R \tag{13}$$

where R is the erosion yield expressed as m^3/atoms.

The standard deviation $\sigma_{\delta,\Delta t}$ of the eroded thickness is the rms of the roughened material surface after being exposed to an AO fluence $F_{\Delta t}$:

$$\sigma_{\delta,\Delta t} = \sqrt{\frac{1}{N}\sum_{i=1}^{N}\left(\delta^i_{\Delta t} - \overline{\delta_{\Delta t}}\right)^2} \tag{14}$$

where N is the number of points where the ablation thickness t, corresponding to the fluence $F_{\Delta t}$, has been measured.

IV. Internal pressure: Evaluation of Erosion Yield *R*

Let us consider a finite prismatic volume of an assigned isotropic material (Fig. 6). From an initial reference configuration, a finite increment of pressure Δp is applied at constant temperature on all of the faces of the elemental volume. Assume that we consider a reference system whose axes are parallel to the sides of the finite prism; the isothermal compressive modulus and the volumetric thermal expansion modulus at constant pressure can be expressed, respectively, as

$$\frac{1}{V}\left(\frac{\partial V}{\partial p}\right)_T = -3\frac{1-2\nu}{E} \tag{15}$$

$$\frac{1}{V}\left(\frac{\partial V}{\partial T}\right)_p = 3\alpha \tag{16}$$

Use of the expressions (15) and (16) yields the following equation for the total ratio of volumetric change:

$$\mathrm{d}V/V = -3[(1-2\nu)/E]\,\mathrm{d}p + 3\alpha\,\mathrm{d}T \tag{17}$$

The internal pressure, or cohesive pressure, χ_i of a substance is defined as

$$\chi_i = \left(\frac{\partial U}{\partial V}\right)_T \tag{18}$$

where U is the internal energy. The partial derivative (18) represents the reaction forces that a solid exhibits when it is subjected to an isothermal volumetric change. These forces are exerted on the external surfaces of the solid volume, so that they can be represented by a pressure: Nevertheless, this pressure also represents a volumetric potential energy density, which yields the cohesion energy of a unit volume of solid matter.

Expanding the partial derivative in Eq. (18) with the expression of the internal energy, together with Maxwell's equation, yields

$$\left(\frac{\partial U}{\partial V}\right)_T = -p + T\left(\frac{\partial p}{\partial T}\right)_V \tag{19}$$

When a transformation at constant volume is considered, the partial derivative of the pressure with respect to the temperature is obtained by Eq. (18), as follows:

$$\left(\frac{\partial p}{\partial T}\right)_V = \frac{\alpha \cdot E}{1-2\nu} \tag{20}$$

Combining Eqs. (18–20) yields the following expression of the internal pressure:

$$\chi_i = -p + \frac{\alpha \cdot E \cdot T}{1-2\nu} \tag{21}$$

As is shown from Eq. (21), the internal pressure is dependent on the actual pressure to which the solid is subjected, as well as on the temperature of the material. When the typical LEO environmental parameters are considered, the external pressure for a material directly exposed to space is very close to zero; therefore, it can be neglected. Because the temperature of the materials varies along the orbit trajectory, the mean internal pressure must be evaluated given different segments of the orbit itself. Details of this calculation will be discussed later.

The values of internal pressure χ_i for 16 materials commonly employed in space structures are reported in Table 2: The data are ordered according to increasing erosion yield R, and they have been evaluated at a temperature of 273 K to develop a preliminary comparison. The typical value for the cohesive density energy is about

Table 2 Internal pressure and reaction yield for metallic and polymeric materials

Material ($T = 273$ K and $p = 0$ Pa)	E, Pa	ν[a]	α, 1/K	χ_i, J/m^3	R, m^3/atoms $\times 10^{30}$
Gold	7.72E+10	0.42	1.44E−05	1.897E+09	0.000
Aluminum	7.10E+10	0.33	2.27E−05	1.294E+09	0.000
Titanium	1.16E+11	0.34	8.90E−06	8.808E+08	0.000
Germanium	1.30E+11	0.30	6.10E−06	5.412E+08	0.000
Al_2O_3	3.66E+11	0.22	7.20E−06	1.285E+09	0.025
Teflon	1.80E+09	0.46	1.30E−04	7.985E+08	0.100
Kynar	2.41E+09	0.34	1.50E−04	3.084E+08	0.600
Graphite	4.80E+11	0.34	2.00E−06	8.190E+08	1.200
Polystyrene	3.00E+09	0.33	7.98E−05	1.922E+08	1.700
Epoxy resin	5.00E+09	0.35	4.38E−05	1.993E+08	2.100
Carbon–epoxy	8.00E+10	0.12	1.00E−05	2.874E+08	2.300
Polysulfone	2.50E+09	0.33	6.01E−05	1.206E+08	2.400
Kapton	2.50E+09	0.34	4.0E−05	6.279E+07	3.000
PEEK	3.50E+09	0.4	2.20E−05	1.051E+08	3.000
Polymethylmethacrylate	2.20E+09	0.33	6.00E−05	1.060E+08	3.100
Tedlar	2.62E+09	0.33	2.50E−05	5.259E+07	3.200
Mylar	3.79E+09	0.35	1.70E−05	5.863E+07	3.300
Polyethelene	2.40E+09	0.34	7.92E−05	1.622E+08	3.300
Silver	7.60E+10	0.37	1.96E−05	1.564E+09	10.500

[a]Poisson modulus of the material.

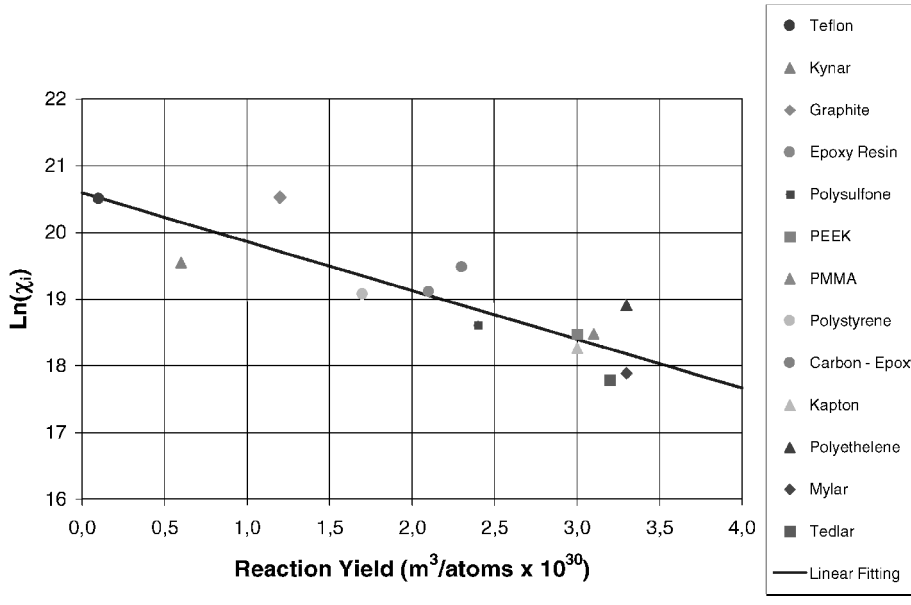

Fig. 8 Logarithm of internal pressure χ_i vs experimental reaction yield R for polymeric materials in LEO.

1 GJ for metallic materials, whereas it is at least one order of magnitude lower, about 100 MJ, for polymers. In Table 2, the internal pressure is also compared to the reaction yields for the different materials. As can be observed, metals and metals oxides, such as Al_2O_3, generally show high internal pressures and very low erosion yields, with the exception of silver. The metals react to AO by developing a film of superficial oxide that can inhibit further chemical reactions; however, the silver oxide does not stick to the metal substrate and so this material can quickly be eroded if exposed to energetic AO. For graphite and organic polymers, the AO combines with the atoms within the polymer chain forming volatile oxides and radicals, such as CO, OH, and NO, thus, producing a superficial erosion. The Teflon® and the carbon–fluorine polymers are only slightly eroded by AO because the C–F bond is very energetic, and the F atoms have a very high electron density, providing an efficient shield for the carbon atoms and their bonds.

For anisotropic materials, such as the carbon–epoxy listed in Table 2, it is impossible to employ expression (21) directly to evaluate the internal pressure because there are different elastic and thermal expansion moduli with respect to the reference frame directions. This problem can be easily avoided if the anisotropic material is composed of two different isotropic phases, as occurs in standard fiber reinforced composites. In fact, in the latter case, it is sufficient to apply the law of mixtures, weighting the cohesive energy density of each phase by its volumetric fraction. The carbon–epoxy data in Table 2 have been estimated under the assumption that the composite is composed of 60% graphite and 40% epoxy resin.

The Monte Carlo simulation is performed by consideration of an interaction energy density ω_i. Because the erosion process involves the formation of volatile or nonsticking oxides, leading to the complete decohesion of the bulk material, it is reasonable to assume that the interaction energy density is equal to the internal pressure of the material because this latter provides an energy scale of the bond interactions among atoms and molecules within a solid phase. Therefore, from now on, it is stated that

$$\omega_i = \chi_i \tag{22}$$

Once the interaction energy density (21) is given, the evaluation of the k_r constant can be performed using Eqs. (12), which relate k_r to the geometric measurings of the profile of the eroded surface, that is, the mean ablated thickness and its rms.

The mean eroded thickness can be assessed by Eq. (13), once the erosion yield R is known. The latter can be evaluated by the use of the linear relation between the internal pressure and the erosion yield itself, as highlighted in Fig. 8. The linear regression

equation is

$$R = -1.3667 \ln \chi_i + 28.1427 \tag{23}$$

where the units of measure are the same as in Table 2.

V. Evaluation of Surface Roughness RMS

The roughness rms can be assessed by profilometric analysis of AO eroded surfaces. Nevertheless, superficial texturing causes strong variations of both the light transmission and friction coefficients of the eroded surfaces. These effects can be very important in evaluating the global changes on the thermal and structural response of materials exposed to the LEO environment. Therefore, an indirect way of evaluating the surface roughness rms of AO attacked surfaces may consist of assessment of the variations of the spectral coefficients related to electromagnetic wave interactions with materials due to superficial scattering, such as transmittance, reflectance, and absorbance.

Following Ogilvy,[20] the changes in spectral transmittance and reflectance for rough surfaces due to multiple scattering can be expressed as

$$t = t_0\left[1 - (2\pi/\lambda^2)(n_1 - n_2)^2\sigma^2\right] \tag{24}$$

$$r = r_0\left[1 - (8\pi/\lambda^2)n_1^2\sigma^2\right] \tag{25}$$

where t is the transmittance, r is the reflectance, n_1 and n_2 are the refractive indexes, λ is the wavelength, and σ is the surface roughness rms. Because σ is not dependent on the reference frame used to evaluate the geometry of surface profile, it can be assumed that

$$\sigma = \sigma_\delta \tag{26}$$

The coefficients t_0 and r_0 refer to the nominal transmittance and reflectance properties for an ideal flat surface. Because the measurements of the refractive indexes are performed in air, it can be assumed that

$$n_1 = 1 \tag{27}$$

whereas n_2 stands for the refractive index of the material. According to Eqs. (24) and (25), both the transmittance and the reflectance of the eroded surfaces diminish with increasing roughness. The relations (24) and (25) are valid if the correlation length of surface roughness is much greater than the wavelength, as will be assumed hereafter. This hypothesis should be verified directly by a profilometric analysis of the eroded surfaces. However, data from in situ missions confirm the latter assumption because a huge reduction of the transmittance coefficient has been highlighted, as will be shown later. Moreover, still following Ogilvy,[20] if the correlation length of the surface roughness were much lower than the wavelength of the incident electromagnetic radiation, both the spectral and total transmittance would increase. It must be observed that Eqs. (24) and (25) represent a solution of Maxwell's equations in the limit of large-scale surface roughness. No approximation related to geometric optics has been introduced.

When a wavelength interval $[\lambda_1, \lambda_2]$ is considered, with λ_2 being much lower than the correlation length of surface roughness, and when the mean transmittances are defined as

$$\overline{t_0} = \frac{1}{\lambda_2 - \lambda_1}\int_{\lambda_1}^{\lambda_2} t_0(\lambda)\,\mathrm{d}\lambda, \qquad \bar{t} = \frac{1}{\lambda_2 - \lambda_1}\int_{\lambda_1}^{\lambda_2} t(\lambda)\,\mathrm{d}\lambda \tag{28}$$

the following relation holds:

$$\bar{t}/t_0 = 1 - 2\pi\tau(n_1 - n_2)^2\sigma^2 \tag{29}$$

where

$$\tau = \frac{\int_{\lambda_1}^{\lambda_2} \frac{t_0(\lambda)}{\lambda^2}\,\mathrm{d}\lambda}{\int_{\lambda_1}^{\lambda_2} t_0(\lambda)\,\mathrm{d}\lambda} \tag{30}$$

Similarly, for the mean reflectances in the spectral range $[\lambda_1, \lambda_2]$,

$$\bar{r}/r_0 = 1 - 8\pi\rho n_1^2\sigma^2 \tag{31}$$

where

$$\rho = \frac{\int_{\lambda_1}^{\lambda_2} \frac{r_0(\lambda)}{\lambda^2}\,\mathrm{d}\lambda}{\int_{\lambda_1}^{\lambda_2} r_0(\lambda)\,\mathrm{d}\lambda} \tag{32}$$

Equations (29) and (31) allow us to evaluate the variations in the mean transmittance and reflectance caused by the surface roughness of the material, with respect to the spectral interval $[\lambda_1, \lambda_2]$. If these properties are measured on flown samples, the surface roughness rms for these properties can be easily assessed. The mean absorbance for the spectral range considered can be simply expressed as

$$\bar{a} = 1 - \bar{t} - \bar{r} \tag{33}$$

As can be deduced from Eqs. (29), (31), and (33), the mean absorbance coefficient increases with surface roughness rms.

VI. Monte Carlo Simulation and Results for Mir and LDEF Exposed Specimens

According to the simulation strategy proposed in this paper, the vertical dimension of the simulation cell h and the reaction constant k_r can be assessed by the mean eroded thickness and the surface roughness rms σ, which, in turn, can be obtained by the internal pressure and the transmittance, or reflectance properties over an assigned spectral range. The simulation provides the evolution of eroded thickness and surface rms by discrete steps of fluence $F_{\Delta t}$, corresponding to time intervals whose duration is Δt. As will be later shown in detail, the exposure to the space environment causes a strong diminution of both the transmittance and reflectance of exposed polymeric samples. This effect is clearly related to surface roughening, as discussed in the preceding paragraph. This implies that the AO exposed surfaces are characterized by the presence of peaks and valleys, whose mean height and depth tend to increase with fluence. On the contrary, the reaction probability p_{rn} has been estimated by the consideration of just one simulation cell layer, instead of the complete array, which is assumed to be representative of the discretized bulk material.

The actual reaction probability for a simulation cell also depends on its positioning with respect to the mean plane of the eroded surface: A cell placed in a deep valley must have a lower reaction probability than an element on a peak because of a complex effect of fluid dynamics shadowing that depends mainly on the geometry of the eroded surface itself. Figure 9 shows qualitatively that the reaction probability p_{rn} of each cell depends on its position along the z axis, that is, on the distance between the cell itself and the plane of the eroded surface.

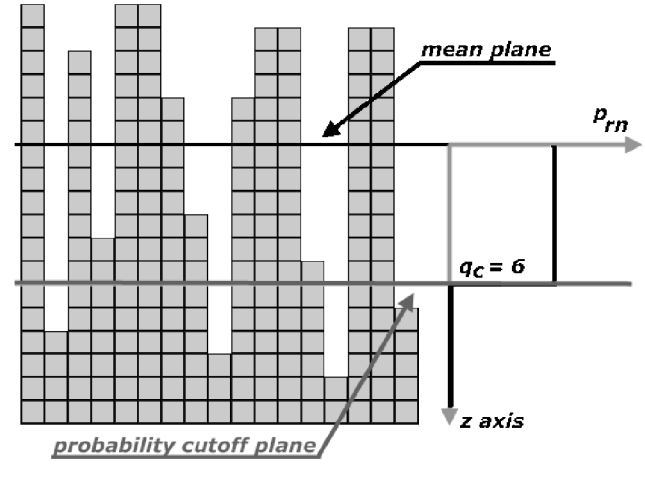

Fig. 9 Reaction probability vs the distance of each simulation cell from the mean plane of the eroded surface.

Table 3 Surface roughness assessed by experimental mean transmittance ratio

Mission	Duration, months	Location	Mean transmittance ratio, final/initial	τ, 1/m^2	σ_δ at the end of the mission, nm
LDEF	10	Trailing edge	0.3205	2.0067×10^{-6}	201.7
LDEF	70	Space end	0.1143	1.9139×10^{-6}	232.5
Mir	28	——	0.0779	1.9381×10^{-6}	233.6
Mir	42	——	0.0390	1.9381×10^{-6}	241.7

To model the effect of surface shadowing, it would be necessary to describe fully the fluid dynamics of rarefied supersonic neutral gas streams interactions with rough surfaces, which represents a problem whose analysis is beyond the scope of this work.

Therefore, to take into account the variation of the reaction probability related to the depth of the exposed simulation cell, a cut-off integer number of cells q_c, measured starting from the mean plane of the eroded surface, is introduced.

When the simulation cell depth ratio is defined as

$$q = (\delta_{ij} - \bar{\delta})/h \tag{34}$$

where δ_{ij} is the ablated thickness corresponding to the cell (i, j) of the simulation array, the following revised definition holds for the reaction probability:

$$p_{rn} = \begin{cases} k_r \exp -\left(2\omega_i \big/ m_0 \overline{v^2} F_{\Delta t}\right) h, & q < q_c \\ 0, & q \geq q_c \end{cases} \tag{35}$$

In view of the preceding discussion, Eqs. (12) for the calculation of the dimension h of the cells and of the constant k_r remain valid if and only if the fluence step $F_{\Delta t}$ is small compared to the total fluence of the mission. Consequently, the depth of the valleys for the initial step of the simulation does not exceed the critical value q_c. When the fluence step $F_{\Delta t}$ is assigned, both q_c and the initial surface rms increment must be set by a proper regression analysis on experimental data, as will be discussed later. Finally, because Eqs. (29) and (31) do not explicitly contain the correlation length of the surface roughness, which is assumed to be much greater than the highest wavelength of the spectral range $[\lambda_1, \lambda_2]$, no estimation can be made of the horizontal dimension d of the simulation cells, for which λ_2 represents only a lower bound.

The Monte Carlo based method for simulating an AO attack on polymeric materials has been applied here to Kapton thin films, which were actually exposed on both LDEF and Mir. Initially, the fluence step $F_{\Delta t}$ has been set to 10^{22} atoms/m^2, which corresponds to variable time intervals, depending on the orbital parameters of the spacecraft, the level of solar activity, and the attitude of the exposed specimens and of the spacecraft itself. Moreover, other assumptions have been introduced for the several parameters that define the operative environment for the missions examined, as follows:

1) The orbital velocity v_{orb} has been set to 8 km/s. This hypothesis is reasonable for both Mir and LDEF, even though in the second case v_{orb} increased during the mission due to altitude reduction.

2) The temperature of neutral gas T_g has been assumed equal to 1000 K, though it can vary slightly due to solar activity and the altitude range of LDEF.

The erosion yield R for Kapton has been set to 3×10^{-30} m^3/atoms, which represents the typical value in the literature. Note that the linear fit (23) of erosion yield vs the natural logarithm of internal pressure provides a value of R equal to 3.2×10^{-30} m^3/atoms, which agrees well with the literature data. Therefore, the mean value of the ablated thickness for the selected fluence step can be evaluated by Eq. (13).

The assessment of the surface roughness evolution step $\sigma_{\delta,\Delta t}$ is much more problematic. The experimental data from Mir and LDEF specimens allows us only to calculate, by inversion of Eq. (29), the surface rms σ_δ at the end of each mission, as shown in Table 3, whereas for Monte Carlo simulation, it is necessary to evaluate the roughness change $\sigma_{\delta,\Delta t}$, corresponding to the selected fluence step.

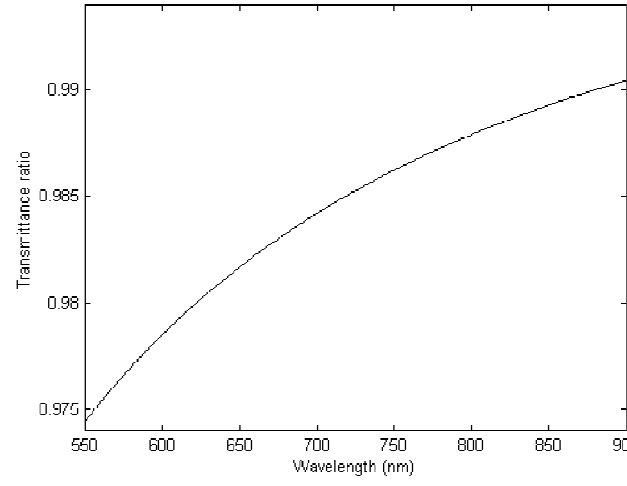

Fig. 10 Effect of a 30-nm initial surface roughness on the transmittance ratio t/t_0 of a 25-μm Kapton film according to Eq. (29).

Moreover, the initial surface roughness and the cutoff number q_c are unknown. All of these parameters must be computed by a nonlinear regression of simulated outputs vs experimental data. To perform this analysis, it has been assumed that the surface roughness, which increases with the fluence step $F_{\Delta t}$, is related to the mean ablated thickness according to the following relation:

$$\sigma_{\delta,\Delta t} = \gamma(\Delta t, R)\overline{\delta_{\Delta t}} \tag{36}$$

where $\gamma(\Delta t, R)$ must be determined by the regression analysis just discussed. The initial value of surface roughness rms σ_δ has been set to 30 nm, which, according to literature, is typical of Kapton thin films.

It must be considered that the transmittance t_0 in Eq. (24) refers to an ideal flat surface, whose rms is zero However, as shown in Fig. 10, the effect of surface roughness limited to a few tens of nanometers on the actual transmittance of the film is very small, and so it can be neglected. Therefore, a small initial surface roughness can be introduced in the simulations without correction of the values of transmittance for virgin films, as listed in Table 1.

The unknown parameters, namely $\gamma(\Delta t, R)$ and q_c, have been evaluated by minimizing the following quadratic function:

$$\Delta(\gamma, q_c) = \sum_{i=1}^{4} \left[\left(\overline{\delta_i^{(\text{sim})}} - \overline{\delta_i} \right)^2 + \left(\sigma_{\delta,i}^{(\text{sim})} - \sigma_{\delta,i} \right)^2 \right] \tag{37}$$

where the subscript i refers to the four values of fluences of in situ missions. The function $\Delta(\gamma, q_c)$ is obtained in a discretized form by varying both $\gamma(\Delta t, R)$ and q_c. Its minimization is simplified because q_c has integer values. From the experimental data concerning both the LDEF and Mir missions, it has been obtained that

$$\gamma(\Delta t, R) = 0.7811, \qquad q_c = 6 \tag{38}$$

and, thus, Eqs. (12) yield

$$h = 4.34 \times 10^{-8} \text{ m}, \qquad k_r = 0.8772 \tag{39}$$

The simulation parameters (38) and (39) are strictly related to the fluence step $F_{\Delta t}$ selected and depend on the material considered, that is, Kapton HN in the present case. However, the fluence step must be much lower than the total AO dose received during the mission; otherwise the agreement between numerical results and experimental data will be poor. Given the different locations of the exposed specimens and their various orientations vs the neutral gas flux, it can be concluded that parameters (38) and (39) identify the Kapton HN interaction with AO for a selected value of fluence step. If this step is varied, parameters (38) and (39) must be reassessed by evaluation of expressions (12) and by minimizing the quadratic function (37). On the other hand, it can be observed that a fluence step set to 10^{22} atoms/m^2 corresponds to the mean irradiation for a sample exposed for 12 h at the leading edge of a spacecraft at an altitude of 500 km and an inclination of 51 deg, during moderate solar activity. Therefore, the selected fluence step can be considered sufficiently small if compared to the AO global irradiation during a LEO flight lasting several months.

The results of the Monte Carlo simulations for the mean eroded thickness, for the surface roughness rms, and for the mean transmittance of the samples are reported in Figs. 11–13.

An orthogonal array of 10^5 simulation cells, providing 200 cells along the x axis (length) and 500 cells along the z axis (depth), has been considered: This number assures a sufficient convergence of the Monte Carlo method for both the mean eroded thickness and the surface roughness rms. Note that both of the results concerning the mean eroded thickness, as well as the surface rms, are in good agreement with the experimental data for LDEF and Mir exposed Kapton films. More precisely, the mean eroded thickness appears to be slightly lower than that calculated by multiplying the erosion yield and the total fluence. This result is clearly related to the introduction of a cutoff for the reaction probability of the simulation cells beneath the mean plane of exposed surfaces. The surface roughness rms reaches an asymptotic value about 249 nm, which corresponds to an almost complete loss of mean transmittance in the spectral range considered here. This trend has already been highlighted by the examination of the Mir and LDEF data, as discussed earlier. From the analysis of the dependence of the simulated transmittance on fluence, reported in Fig. 13, note that the values of the mean transmittance for exposed Kapton are slightly underestimated for fluences exceeding 3×10^{24} atoms/m^2. This low accuracy can be related to threshold sensibility of the spectrophotometer employed for the experimental surveys on flow films. However, again from Fig. 13, it is clear that the AO attack seriously affects the spectral properties of exposed Kapton for fluences exceeding 5×10^{23} atoms, due to the increased surface roughness. As is shown by Eqs. (31) and (33), this effect strongly raises the absorbance of the kapton films during flight and, therefore, it must be taken into account in the design stage.

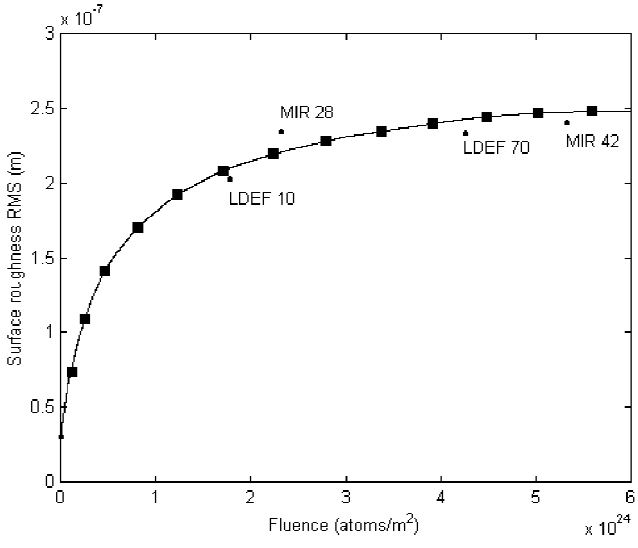

Fig. 11 Surface roughness rms: comparison between Monte Carlo simulation results and experimental data.

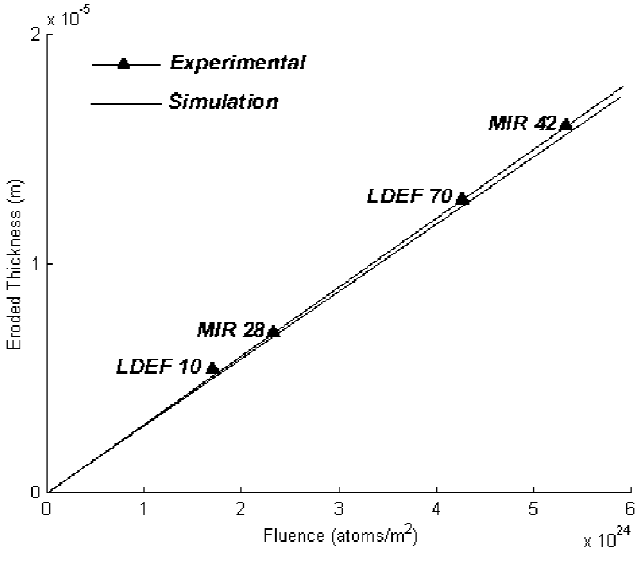

Fig. 12 Eroded thickness: comparison between Monte Carlo simulation results and experimental data.

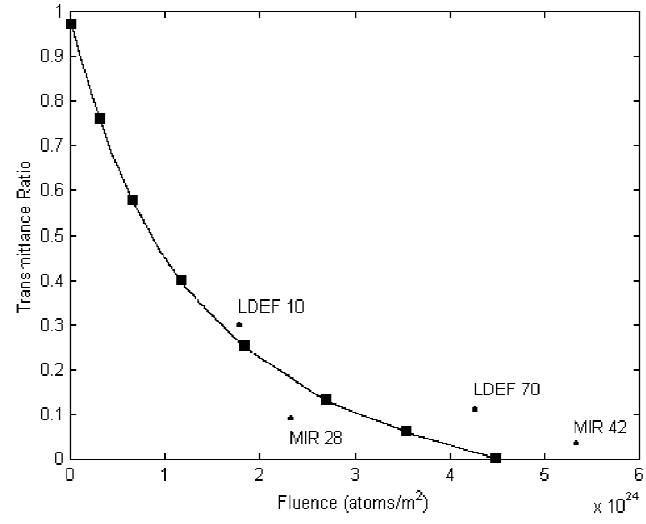

Fig. 13 Mean normal transmittance in the spectral range (550–900 nm): comparison between Monte Carlo simulation results and experimental data.

VII. Conclusions

A Monte Carlo based approach to simulating the AO attack on polymeric films exposed to the LEO space environment has been presented and discussed. The basic assumption is that the bulk material can be represented by an array of finite volume simulation cells, whose probability of being eroded is given in a standard exponential form, relating the total amount of kinetic energy stored by an AO flux in each simulation volume and the internal pressure of the material itself. It has also been shown that the erosion yield R is almost a linear function of the logarithm of the internal pressure for polymeric materials. This observation has presented the possibility of development of a tool to estimate the erosion yield of polymeric materials, starting from their thermomechanical properties.

The pronounced diminution in the mean direct transmittance in thin Kapton films has been related to surface roughening, via the standard scalar equation of electromagnetic wave surface scattering. This observation has allowed us to calculate the surface rms for Kapton films exposed to the space environment on both LDEF and Mir, in the range between 550 and 900 nm. The Monte Carlo approach proposed here requires an input of the mean eroded thickness

and the surface roughness rms, corresponding to an assigned fluence step of AO. These parameters have been calculated for LDEF and Mir exposed Kapton specimens by a nonlinear regression on experimental data. The outputs of the simulations are the mean eroded thickness, the surface roughness rms, and the mean direct transmittance for the spectral range, considered as functions of the total AO fluence. Comparison between the results of the simulation and the experimental data evidences good agreement for all of the parameters taken into consideration. Hence, the proposed method can represent a valid tool to estimate the Kapton response to space environment exposure in terms of both mass loss and degradation of spectral properties. The approach presented here can be employed for other polymers, provided that the spectra of exposed specimens are available. Further investigation is necessary to establish the reliability of the proposed method for space-employed materials, especially in the field of passive thermal control of spacecraft, such as thermal blankets and sunshields.

References

[1]Banks, B. A., "Atomic Oxygen," *Proceedings of the LDEF Materials Data Analysis Workshop*, NASA CP 10046, 1990, pp. 191–216.

[2]Stein, B. A., and Young, P. R. (eds.), *LDEF Materials Workshop 91*, NASA CP 3162, 1992, Pt. 1, pp. 59–71; Pt. 2, pp. 515–593.

[3]Stein, B. A., and Young, P. R. (eds.), *LDEF Materials Workshop 92*, NASA CP 3194, 1993, Pt. 1, pp. 437–456; Pt. 4, pp. 675–712.

[4]Startsev, O. V., and Nikishin, E. F., "Ageing of Polymeric Composite Materials in Outer Space," *Mechanics of Materials*, Vol. 29, 1993, pp. 457–467.

[5]Koontz, S. L., and King, G., "Intelsat Solar Array Coupon Atomic Oxygen Flight Experiment," *Journal of Spacecraft and Rockets*, Vol. 31, No. 3, 1994, pp. 475–481.

[6]Arnold, G. S., and Peplinski, D. R., "Reaction of Atomic Oxygen with Vitreous Carbon Laboratory and STS-5 Comparisons," *AIAA Journal*, Vol. 23, No. 6, 1985, pp. 673–683.

[7]Akishin, A. I., and Novikov, L. S., *Simulation Methods for the Effect of Space Environment on the Spacecraft Materials*, MGU Press, Moscow, 1986, Chaps. 1 and 3.

[8]Koontz, S. L., Leger, L. J., Albin, K., and Cross, J., "Vacuum Ultraviolet Radiation/Atomic Oxygen Synergism in Materials Reactivity," *Journal of Spacecraft and Rockets*, Vol. 27, 1990, pp. 346–348.

[9]Allegri, G., Lecci, U., Marchetti, M., and Poscente, F., "On the Reliability of Skin-Core Bonding Joint in Sandwich Materials for Space Structures," 52nd International Astronautical Conf., IAF-01-I.6.05, International Astronautical Federation, Toulouse, France, Oct. 2001.

[10]Koontz, S. L., Leger, L. J., and Rickman, S. L., "Oxygen Interactions with Materials III—Mission and Induced Environments," *Journal of Spacecraft and Rockets*, Vol. 32, No. 3, 1995, pp. 475–482.

[11]Silverman, E., "Space Environmental Effects on Spacecraft: LEO Materials Selection Guide," NASA CR 4661, 1995.

[12]Heynderickx, D., "ESA's Space Environment Information System (SPENVIS): A WWW Interface to Models of the Space Environment and Its Effects," AIAA Paper 2000-0371, Jan. 2000.

[13]Heynderickx, D., "SPENVIS—Space Environment Information System," URL: http://www.spenvis.oma.be/spenvis/atomox_par.html [cited 20 Jan. 2002].

[14]Ferguson, D. C., "The Energy Dependence of Surface Morphology of Kapton Degradation Under Atomic Oxygen Bombardment," *Proceedings 13th Space Simulation Conference*, NASA, Washington, DC, 1984, pp. 205–215.

[15]De Groh, K. K., and Banks, B. A., "Atomic Oxygen Undercutting of Long Duration Exposure Facility Aluminized Kapton Multilayer Insulation," *Journal of Spacecraft and Rockets*, Vol. 31, No. 4, 1994, pp. 656–664.

[16]Snyder, A., "Investigation of Atomic Oxygen Erosion of Polyimide Kapton H Exposed to a Plasma Asher Environment," NASA TM-1999-209178, 1999.

[17]Banks, B. A., Stueber, T. J., and Norris, M. J., "Monte Carlo Computational Modeling of the Energy Dependence of Atomic Oxygen Undercutting of Protected Polymers," *Proceedings of the 4th International Space Conference on Protection of Materials and Structures from the LEO Space Environment*, Inst. for Aerospace Studies, Univ. of Toronto, Toronto, 1998, pp. 1–10.

[18]Snyder, A., and Banks, B. A., "Fast Three-Dimensional Method of Modeling Atomic Oxygen Undercutting of Protected Polymers," NASA TM 2002-211578, 2002.

[19]Milinchuk, V. K., and Smirnova, T. N., "Properties of the Polymeric Films after Natural Exposure to the Space Environment on the Orbital Space Station MIR," *Proceedings of the 8th Symposium on Materials in a Space Environment*, ESA, Noordwijk, The Netherlands, 2000, pp. 104–114.

[20]Ogilvy, J. A., *Theory of Wave Scattering from Random Rough Surfaces*, Adam Hilger, Bristol, England, U.K., 1991, Chap. 2.

G. V. Candler
Associate Editor